JOURNAL OF SPACECRAFT AND ROCKETS
Vol. 32, No. 4, July–August 1995

# VLF Wave Experiments in Space Using a Modulated Electron Beam

W. John Raitt*
*Utah State University, Logan, Utah 84322-4405*
James Ernstmeyer† and Neil B. Myers‡
*U.S. Air Force Rome Laboratory, Hanscom Air Force Base, Massachusetts 01731*
A. Brent White§
*Utah State University, Logan, Utah 84322-4140*
Susumu Sasaki,¶ Koh-Ichiro Oyama,** and Nobuki Kawashima††
*Institute of Space and Astronautical Sciences, Sagamihara Kanagawa 229, Japan*
Anthony C. Fraser-Smith‡‡
*Stanford University, Stanford, California 94305-4055*
Brian E. Gilchrist§§
*University of Michigan, Ann Arbor, Michigan 48109-2143*
and
Thomas J. Hallinan¶¶
*University of Alaska, Fairbanks College, Alaska 99701*

**A sounding-rocket payload to study the generation and emission of electromagnetic waves from a modulated electron beam was developed and successfully flown from the Poker Flat Research Range, Alaska, in March 1992 on a Black Brant 11 sounding rocket. We describe the mission objectives, the instrumentation, flight operations, and preliminary results from the flight. The payload contained a modulated electron gun with a triode arrangement of electrodes allowing modulation of the beam current up to vlf frequencies. Vehicle charging was inhibited by a gas-release system, synchronized with the beam emissions. A network of ground stations was set up to try to receive signals from the modulated beam, and low-light systems were set up to look for evidence of the beam below the payload trajectory. No evidence of beam-induced wave radiation to the ground was detected. However, strong vlf frequencies following the preset program were clearly detected by the diagnostic free flyer and the tethered daughter payload segment. The effect of the gas releases was very marked. The vehicle potential dropped from over 1 kV to about 30 V when the gas was turned on. Some evidence of the light from beam–atmosphere interactions was seen near the end of the flight, but in general, the optical results were not very informative. The launch was successful, mission operations were as planned, and good-quality onboard data were collected throughout the operational part of the flight.**

## Introduction

ELECTRON-BEAM experiments from a variety of space platforms have been performed since it was shown experimentally in the early 1960s that the theoretical prediction of severe limits on the beam current resulting from vehicle charging was incorrect, and emission currents of about 100 mA were possible from sounding-rocket payloads at low earth orbit (LEO) altitudes.[1,2] The earlier experiments were primarily directed towards using beams as magnetospheric probes, as in the ECHO series,[3] or studying beam–environment interactions as in the SCEX, ARAKS, POLAR, and CHARGE series.[4–8] One of the results of the beam–environment interaction is to trigger plasma instabilities with the consequent emission of wave energy in various modes even from constant-current beams.[9] The use of a current-modulated electron beam as an antenna to launch vlf waves was initially reported by Holtzworth and Koons, who found that a 4-kV electron beam with 80-mA current modulated at 3 kHz did emit waves, which were detected by a separated free-flying package.[10] Limited experiments on wave emission from modulated electron beams were performed in the CHARGE series, but the receiver was always tethered to the beam-generating platform until the CHARGE-2B flight reported in this paper.

A collaborative program between the U.S. and Japan to study electron-beam–space-system interactions using a tethered mother–daughter payload configuration was initiated by the Tethered Payload Experiments program (TPE), which started with two Japanese payloads on flights K-9M-69 in 1980 and S-520-2 in 1981. Two U.S. flights, designated Cooperative High Altitude Rocket Gun Experiments (CHARGE-1 and CHARGE-2), flown from White Sands Missile Range, followed in 1983 and 1985, respectively.[7,8] System problems resulting in limited tether deployment and/or prime-power-supply failures plagued the early flights. The addition of in-line thrusters to the daughter on CHARGE-1 solved the problem of limited tether deployment, but again a power-source problem defeated the achievement of the prime objectives of the flight. The first comprehensively successful payload was CHARGE-2. The latest in the series of joint U.S.–Japan collaborative sounding-rocket payloads, CHARGE-2B, was launched on March 28, 1992, from

Received Jan. 15, 1993; revision received Jan. 25, 1994; accepted for publication Nov. 25, 1994. 

*Professor, Center for Atmospheric and Space Sciences. Member AIAA.
†Electronics Engineer, USAF Rome Lab/ERCP.
‡Research Physicist, USAF Rome Lab/ERCP. Member AIAA.
§Systems Engineer, Systems Division, Space Dynamics Laboratory.
¶Associate Professor, Research Division for Space Applications, 3-1-1 Yoshinodai.
**Associate Professor, Research Division for Planetary Science, 3-1-1 Yoshinodai.
††Professor, Research Division for Planetary Science, 3-1-1 Yoshinodai.
‡‡Professor, Departments of Electrical Engineering and Geophysics.
§§Assistant Professor, Electrical Engineering and Computer Sciences, Space Physics Research Laboratory. Member AIAA.
¶¶Professor, Geophysical Research Institute.

Poker Flat Research Range (PFRR), Alaska, USA, using a Black Brant 11 booster rocket.

Two common themes of the TPE series have been the study of the charging of a space platform resulting from the emission of an electron beam, and the utilization of a section of the payload deployed from the beam platform, but electrically connected by an insulated conducting wire tether, to carry diagnostic instruments and to provide a reference against which to measure the electrical potential of the beam platform.

CHARGE-2B conformed to the general characteristics described above, but was enhanced by the addition of a second part of the payload, the Diagnostic Free Flyer (DFF), an autonomous system, released from the beam platform early in the flight. The DFF was instrumented to provide data on wave fields, on ambient ionospheric electron density, and on vehicle attitude using a three-axis magnetometer. The tethered segment of the payload was instrumented with the tether deployment system, HF and vlf receivers, a charge probe, and a tether current monitor. Although CHARGE-2B included the platform electrical-charge-monitoring capability of the earlier flights in the series, the prime objectives were oriented to the generation and propagation of vlf waves from a modulated electron beam. The vehicle potential measurements were used to enable the emitted energy of the electron beam to be determined as an aid in modeling the wave-generation predictions for the electron beam. The other main difference of the CHARGE-2B payload was the much increased electron-beam current and electron energy over the earlier flights in the series. The peak beam current was approximately 2 A, and the emitted electron energy was 3 keV, compared to the 80-mA, 1-keV beam on the earlier CHARGE flights. The high beam current dictated the need for an active method of preventing the payload from becoming charged up to potentials high enough to inhibit the electron-beam emission. On the basis of previous serendipitous experience of the effect of the gas jets associated with the attitude control system (ACS) in lowering the impedance of the electrical connection between charged sounding-rocket payloads to the ionosphere, we used a gas-release system synchronized to the electron-beam firings to clamp the vehicle at a low potential. To test the effectiveness of this system, and to allow the possibility of beam emission at two different energies relative to the space environment, we alternately used and inhibited the gas-emission grounding scheme during the beam emission program.

CHARGE-2B was scheduled for launch at PFRR for reasons related to siting of ground-based vlf receivers, recovery of payload components, and the need for a large range area to accommodate the dispersion of the landing location of the new Black Brant 11 booster configuration. The auroral-zone location of PFRR was potentially a disadvantage for other aspects of the mission, particularly the low noise levels required for the ground-based receivers, and the low background illumination needed by a ground-based low-light-level television (LLLTV) system searching for evidence of the beam trace below the rocket trajectory. We were able to take advantage of existing instrumentation installed at PFRR to continuously monitor auroral activity for the low levels needed. The payload was launched at 10:27 p.m. local time (07:27 UT) on March 28 (March 29 UT), 1992, into clear skies with a diffuse auroral background illumination of about 2 kR, no arcs to the north of the launch site, and a weak, low-intensity, diffuse arc to the south. The booster underperformed slightly, lifting the payload to an apogee of 266 km, 2.3$\sigma$ low from the predicted apogee of 285 km. The reduced flight time resulting from the lower apogee prevented completion of the final attitude maneuver at high enough altitude to prevent arcing of the electron guns. However, since this was a repeat of an earlier maneuver, the attitude component of the flight plan was not omitted, but there was a loss of altitude variability at that attitude. All mechanical and electrical systems worked well, as did the science instruments. The ACS program performed as planned, and the payload was tracked by radar throughout the useful portion of the flight. Recovery of the two tethered segments of the payload was accomplished successfully. The deployed tethered section was in very good condition, but the beam platform suffered serious heat damage during re-entry, before parachute deployment.

In this paper we will describe the payload instrumentation and support systems, summarize the mission plan, and present some preliminary results from both the flight instruments and the ground support instrumentation.

## Mission Objectives

The prime objective of the CHARGE-2B mission was to determine if a medium-energy electron beam modulated at vlf frequencies could generate electromagnetic waves that would propagate from LEO altitudes to the surface of the earth. A secondary objective was to determine if the potential of the beam platform relative to the ionosphere during beam emission would be controlled to a low value during the operation of a gas-release grounding system.

Instrumentation was provided and deployed in space such that the source function of the waves from the modulated beam, the beam-platform potential, and the near-field wave characteristics could be determined. The gas-release-system emission program allowed studies of the dependence of wave generation on beam particle energy, which varied according to whether the beam was emitted from an electrically charged or discharged beam generator platform. The effect of beam pitch angle on the wave generation was studied by using a programmed attitude control system. Instrumentation was deployed on the ground to attempt to receive the vlf electromagnetic waves from the beam, and also to search for optical aurorae produced at E-region heights by the electron beam.

## Payload

### Mother

*Modulated Electron Gun (MEG)*

The purpose of the MEG was to generate a current-modulated electron beam. A nominal peak beam current of 2 A at a beam electron energy of 3 keV was achieved by connecting two 1-A MEG units in parallel, with a synchronizing interconnection between their respective modulators.

The electrostatic elements of the electron guns consisted of a 0.25-in.-diam planar, disk-shaped filament formed from a serpentine arrangement of a thin tungsten wire; a perveance anode mounted close to the filament to control the beam current; and an accelerator anode to provide the acceleration of the beam to the desired electron energy. An axial magnetic field produced by a coil surrounding the electrostatic elements limited the divergence of the beam to about 5 deg full width. Figure 1 illustrates the geometry of the electron optics.

Rogowski coils surrounding the beams of each MEG measured the emitted beam current. The beam-current sampling circuit was configured to measure the peak beam currents in the negative and the positive sense during the interval between telemetry samples at 5000 $s^{-1}$. These two signals were used to determine the peak emitted current of the sinusoidally modulated beam.

The electrical energy to accelerate the beam particles was provided by a battery of NiCd rechargeable cells. The battery was constructed of ten 300-V modules connected in series, each having a relay disconnect.

The modulating voltage to control the beam current was amplified to the correct level of close to 3000 V by a vacuum-tube amplifier

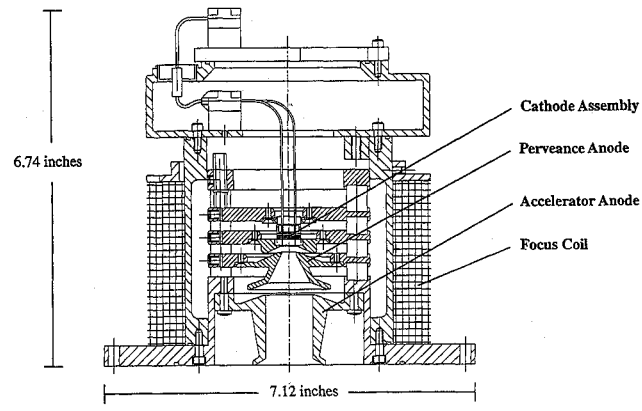


**Fig. 1 General assembly of electrodes in the MEG accelerator.**

mounted in the MEG enclosure. For the CHARGE-2B application, the signal for the modulation amplifier was derived from a frequency synthesizer that generated a waveform calculated to result in a sinusoidal variation of beam current after being modified by the transfer characteristic of the electron gun. The frequency synthesizer was programmed to generate a sequence of four triads of frequencies in the vlf band. Each triad was composed of a frequency grouping consisting of a 180-Hz offset below a center frequency, the center frequency, and a 180-Hz offset above the center frequency. The nominal center frequencies were 4.5, 9.0, 14, and 18 kHz. Figure 4 in the next section shows the measured frequencies and a diagram of the timing of the frequency-synthesizer program.

*Vehicle Potential*

The electrical potential of the mother payload relative to the ambient ionosphere was determined by measuring the voltage between the end of the tether penetrating the mother section and the ground reference of the mother. The input impedance of the voltage-measuring circuit was 10 MΩ, so it could be assumed that the deployed daughter was close to ionospheric potential. Thus, the voltmeter gave a direct reading of the mother electrical potential relative to the daughter and hence to the ionosphere.

Since the beam was modulated at vlf frequencies, it was expected that the mother potential would also be modulated. It was not possible to include a high-speed data-sampling system, so a peak-voltage monitor circuit was incorporated in the voltmeter. The peak voltage in the interval between telemetry samples was returned from the instrument. Four separate logarithmic channels sampled the peak potential for the positive envelope, and four separate logarithmic channels for the negative envelope. The moduli of the upper limits of the ranges were 4 kV, 2 kV, 1 kV, and 100 V. Each channel was sampled 5000 times per second.

The monitors were very stable, and cross comparisons between the outputs of the different ranges were very close. However, a failed protection diode on the input of one negative channel resulted in a saturation level of ≈1.8 kV for each of the two lower-sensitivity negative potential ranges.

*Gas-Release System*

The gas-release system consisted of an argon gas supply that was released into the ionosphere using two pairs of opposed nozzles emitting tangentially to the mother skin in a direction perpendicular to the longitudinal axis of the rocket. The emission of the gas was controlled by a valve whose operation was synchronized with alternate groups of beam firings by the payload science controller. The total emission rate of the gas discharge system was 0.2 mole/s. The pressure at the nozzles was reduced to 150 psi by a pressure regulator from the gas-tank pressure of 4500 psi.

The gas system operated correctly throughout the flight. It also performed its function of reducing the vehicle–ionosphere potential very well at all altitudes and attitudes achieved by the payload. The released gas did not adversely affect the operations of the MEGs by causing localized discharges or arcs in the vicinity of the MEG electrodes.

*Charge Probe*

A dielectric charge probe was included in the payload as an alternate method of monitoring changes of mother potential when the electron beam was firing. The sensor consisted of a Teflon dielectric covering a metal plate with dimensions 50 × 100 mm.

*Payload Controller*

Because of the high voltages and power levels existing in the CHARGE-2B payload, it was decided not to use computer control of the science experiments. A hardened system was developed using a mechanically driven optical-disk encoder marked to generate addresses used to extract information from a table stored in an EEPROM memory module. One complete cycle of scientific modes took 32 s, and so the disk was geared to rotate once every 32 s to produce a program that was continuously repeated throughout the flight.

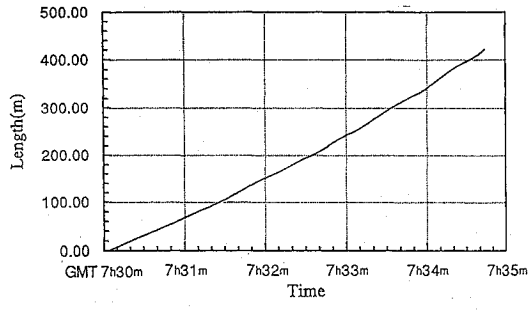


**Fig. 2 Plot of tether length against Universal Time for the section of the flight during which the tether was being deployed.**

**Daughter**

*Tether Deployment System*

The tether deployment system is a mechanism that allows the tether wire to be deployed in a direction parallel to the axis of rotation of the spool. The spool contained 426 m of wire made of a stainless-steel conductor coated with Teflon having an outside diameter of 0.66 mm. The total electrical resistance of the wire was 4000 Ω. The deployment length was monitored with a resolution of 0.1 m. The deployment system worked well during the flight, and a plot of the length of tether deployed as a function of time is shown in Fig. 2. The initial deployment speed was 1.2 m/s with an increasing trend to an average final separation speed of 1.8 m/s. Speed fluctuations at the 30-s period of the daughter thruster jet operation, showing increasing amplitude as the flight progressed, were superimposed on the general trend of the separation speed.

*HF Receiver*

The HF wave detection system consisted of a 2.4-m tip–tip dipole connected to a receiver. The frequency to which the receiver was tuned was swept from 0.2 to 10 MHz with a period of 250 ms, maintaining a constant bandwidth of 200 kHz. The dynamic range of the receiver was 48 dB with a maximum sensitivity of 5 mV. The receiver was calibrated for 0.75 s every 40 s by an internal 1-MHz oscillator.

*vlf Receiver*

Another 2.4-m tip–tip dipole antenna perpendicular to that used for the HF receiver was used to provide an input signal for a vlf receiver. The vlf receiver detected signals in the broad band of 0.5–30 kHz, with a maximum input level of 1 mV rms. The wideband vlf signal was telemetered to the ground using FM–FM modulation of a dedicated S-band telemetry link.

*Charge Probe*

A dielectric charge probe of the same type as that included in the mother section of the payload was retained in the daughter section of the payload.

**DFF**

The DFF was one of the three autonomous subpayloads that flew as part of the CHARGE-2B sounding-rocket mission. The DFF carried electric and magnetic wave detectors, as well as a Langmuir probe. The DFF was not tethered, and its trajectory relative to the mother was such that its relative motion was downward, approximately parallel to the geomagnetic field. It provided wave measurements complementary to those planned for the daughter receivers and the vlf ground stations.

*Waves-and-Fields Experiment*

*Electric field measurements.* The DFF electric field experiment consisted of four spherical, carbon-coated sensors supported in a tetrahedral configuration by fiberglass booms deployed at 45 deg to the spin axis of the payload. All sensors were deployed to a perpendicular distance of 0.8 m from the DFF spin axis. Consequently, there was no chance that any of the sensors was magnetically shadowed by the payload structure during the flight.

A sum-and-difference scheme was employed by the onboard electronics to obtain all three components of the electric field. The $X$ and $Y$ axes were approximately perpendicular to the **B** field, making the $Z$ axis approximately field-aligned. The sensor separation was 1.51 m along the $X$ and $Y$ axes, and 0.77 m along the $Z$ axis. The $X$-axis sensors contained HF preamplifiers, allowing the $X$ component of fluctuating electric fields to be measured at frequencies up to 30 MHz. The $Y$-axis sensors were sensitive only up to 100 kHz. All sensors responded to potentials induced by dc electric fields.

Onboard processing of the electric field signals produced five separate classes of outputs: dc electric potentials, dc electric fields, broadband electric waves, four-channel filtered wave power, and HF swept frequency analyzer spectra.

*Magnetic wave experiment.* A triaxial search-coil antenna was used to detect fluctuating magnetic fields. The antenna employed paired coils, loaded with high-permeability cores. A high-gain preamplifier was located in the search-coil housing. No frequency equalization scheme was used. As a result, the sensitivity of all three channels improved linearly with frequency over the 0- to 50-kHz range of interest. A resonance due to intrawinding capacitance occurred at close to 100 kHz.

The instrument was mounted on a nonconductive fiberglass structure under the nose tip to minimize the influence of spacecraft-generated interference on the search coil. This structure placed the search coil at least a meter away from any other experiment electronics, and eliminated current loops in the support structure.

*Langmuir Probe*

The Langmuir probe flown on the DFF was of the gridded spherical type. The diameter of the grid was 2.54 cm, and that of the solid concentric collector, 1.68 cm. The grid potential relative to the DFF skin was swept linearly from −3 to +5 V and back in one second. It was then held at +3 V for one second, and finally held at 0 V for two seconds. This sweep program was maintained throughout the flight. Throughout the sweep, the center collector was held at a positive potential of 20 V with respect to the grid to suppress secondary electron emission, and to ensure that virtually all electrons passing through the grid were collected. The effective grid transparency to electrons was estimated to be 80%.

The Langmuir probe was deployed in the spin plane at a distance of 40.6 cm from the DFF spin axis. The probe was magnetically shadowed by the aft end of the DFF payload skin for as much as 10 deg of payload rotation every spin period. Minor effects due to this shadowing were observed at positive probe bias potentials.

**General Configuration**

*ACS*

The mother payload was attitude-controlled in three axes by a cold-gas attitude control system. The operating gas was nitrogen. The gas jets provided an alternate grounding scheme for the payload if they operated when the gas release system was off and the electron beam was on. The jets only operated for a few hundred milliseconds, and when they were on, the gas was released in a pulsed mode with a pulsing frequency of about 10 Hz.

*RCS*

On the basis of experience from earlier flights of the CHARGE mother–daughter configuration, it was decided to use a reaction control system to stabilize the daughter in pitch and yaw and to compensate for possible tipoff at mother–daughter separation. The roll-axis control jets were reoriented and used to produce thrust in a direction to separate the daughter from the mother. The operation of the jets was determined by an intervalometer providing 3 s of thrust at 30-s intervals. The gas used in this system was again nitrogen.

*Vehicle Service Modules*

The provision of power, telemetry, and mission timing control was provided by three separate vehicle service modules included in the mother, daughter, and DFF elements of the payload. The mother used a PCM digital telemetry system communicating at 800 kb/s, and the daughter used another PCM system with a capacity of 400 kb/s and an FM–FM system to return wideband signals from the vlf receiver. The DFF had an additional telemetry link operating at 800 kb/s. General payload power was provided by rechargeable NiCd battery packs operating at a nominal voltage of 28 V. All segments of the payload were controlled by electronic timers with a time resolution of 0.1 s.

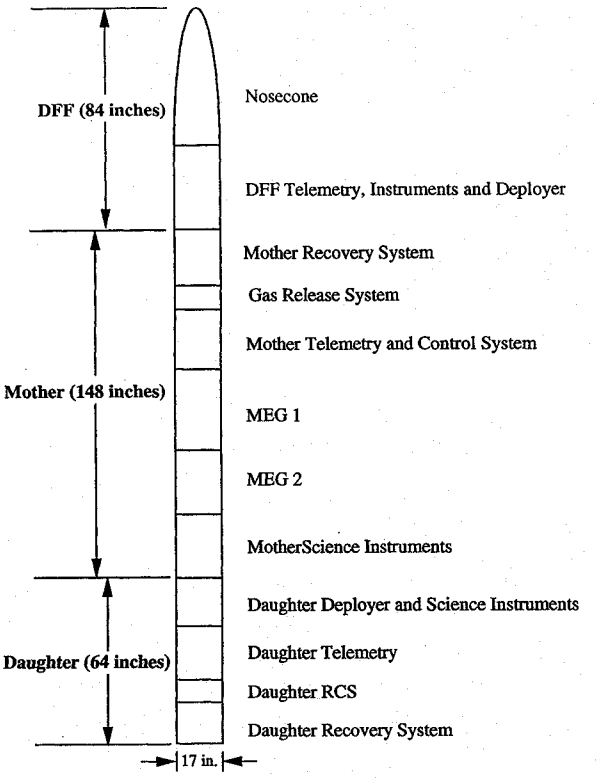


**Fig. 3 Drawing of the payload buildup showing the positions of the various subsystems in the launch configuration.**

*Recovery Systems*

The mother and daughter segments each had parachute recovery systems. The parachutes operated correctly for each segment, and the payload sections were recovered. Unfortunately, the re-entry attitude of the mother was such that prior to parachute deployment, severe heating damage occurred for the mother science section and the cables passing through a raceway external to the pressurized sections of the MEG modules. The daughter was recovered in excellent condition.

*Payload Arrangement*

The payload sections were stacked as shown in Fig. 3. The space under the nose cone and the first parallel section housed the DFF and its deployment mechanism. This was followed by the individual sections of the mother, which were in turn followed by the individual sections of the daughter. The overall length of the payload was 296 in., making it the longest Black Brant payload flown up to that time. The extreme length and the flexibility resulting from the large number of joints caused some early concerns about the stability of the payload during the powered section of the flight, but final computations and the actual flight data did not show any evidence of significant stability problems.

## Mission Profile

**Launch Window**

The launch windows were determined by several considerations:

1) Moon and sun at least 15 deg below the horizon at apogee: a) to provide dark viewing for beam detection from the ground and b) to avoid photoemission effects on the DFF electric field probe.

2) No clouds.

3) No bright auroral forms along the flight trajectory projection to auroral emission altitudes: a) to provide dark viewing for beam optical detection at the ground and b) to avoid the possibility of local

ionospheric disturbance due to particle precipitation and/or strong magnetospheric convection electric fields.

4) Low local electrojet activity, to avoid interference by ionospheric electric fields driving the electrojet.

The determination of suitable local conditions and a real-time forecast of approaching auroral activity was greatly helped by the many data streams of both remote and local conditions flowing into Poker Flat Research range, and displayed on an array of monitors.

In practice, for the late March period chosen for the flight, the restrictions led to launch after about 10:25 p.m. local time until about 2:00 a.m. on the next day for a ten-day period around the new moon.

### Science Timeline

The science timeline consisted of a basic sequence of emission frequencies with the gas-release system on or off. This sequence was repeated throughout the flight, and provided a combination of a given frequency of emission at a range of altitudes and attitudes, and with the vehicle grounded by the gas-discharge system or electrically floating when the gas-discharge system was off.

The modulation frequency sequence consisted of four basic frequencies, 4.47, 8.97, 14.01, and 17.94 kHz, with an offset of ±0.18 kHz used to shift each of the basic frequencies. Thus for a given frequency period a triad of frequencies was emitted in the sequence $f_0 - \Delta f$, $f_0$, $f_0 + \Delta f$, where $f_0$ is the basic frequency listed above. Each frequency was emitted for 0.8 s with a 1-s gap after each triad. Two triads at the same basic frequency were emitted in succession, one with the gas-release system on, and one with it off. Figure 4 illustrates the complete 32-s science sequence diagrammatically.

### Trajectory

*Mother*

The rocket was launched with an azimuth of 5.75 deg and reached an apogee of 266 km. There was a drift in azimuth of about 1 deg during the flight. The altitude profile is shown in Fig. 5. The figure shows the initiation times and durations of the ten frequency program sequences executed during the flight.

*Daughter*

The daughter trajectory was essentially the same as that of the mother, except it was deployed in a magnetically westward direction at a mean speed of 1.5 m/s. The speed fluctuated because of the periodic thrust given by the RCS jets, but by the time the tether was cut, it had deployed to its full length of 426 m.

*DFF*

The sequence of flight events for the DFF began with nose-cone deployment that exposed the DFF antennas and Langmuir probe, which were then deployed 10 s later. The separation of the DFF from the main payload with a relative speed of 5.3 m/s occurred after a further delay of 33 s. The payload was spinning at 1.105 rps at separation. The DFF continued to spin stably about its spin axis at the same rate throughout the flight. The trajectory of the DFF followed that of the mother, but with an increasing separation.

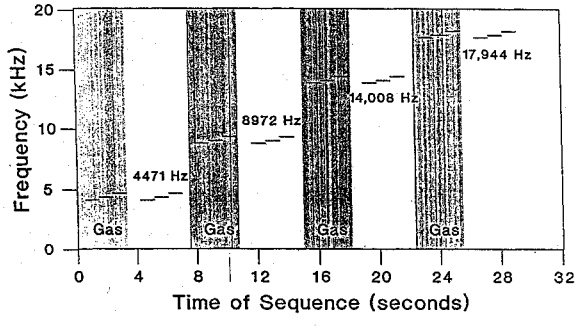


**Fig. 4 Diagram of the frequency program and gas-release program for one of the flight sequences. The emission frequencies shown are the center frequencies of each triad, the deviations being ± 180 Hz.**

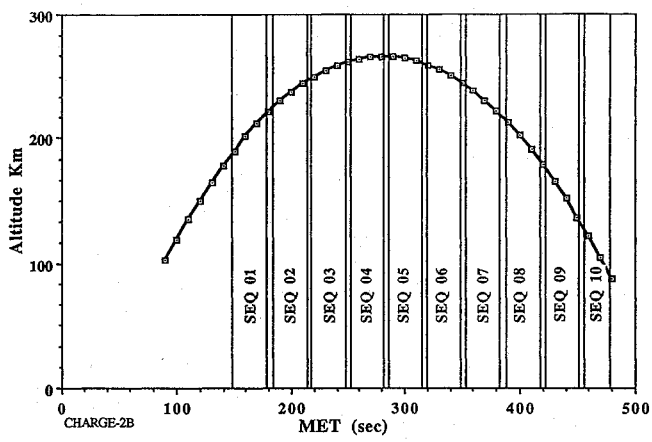


**Fig. 5 Measured flight altitude trajectory, showing the periods during which each of the sequences was executed.**

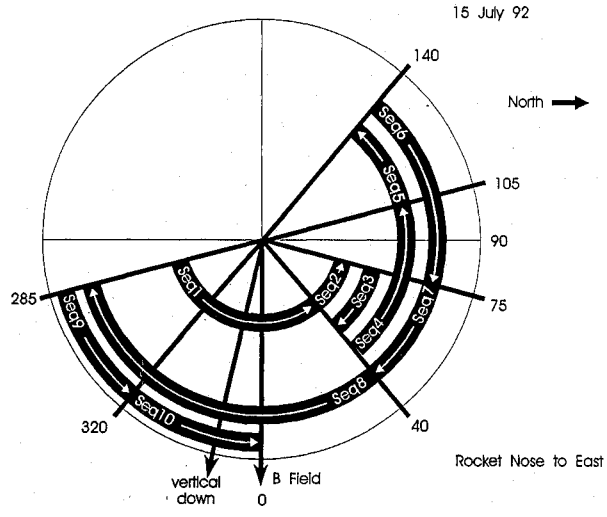


**Fig. 6 Diagram illustrating the pitch-angle scans of each of the flight sequences. The angles shown are actual pitch angles, and the scan rates were adjusted to accomplish the varying angular scans in the same 32-s time interval for each beam–gas sequence.**

The direction of the DFF velocity vector was downwards and at about 6 deg from being parallel to the geomagnetic field. The useful part of the flight lasted about 400 s after DFF separation, by which time it was located at a distance of ≈2 km from the mother payload.

### Attitude Plan

The initial attitudes planned for the payload were to achieve deployment of first the DFF, and then the daughter, in the desired directions. Following orientation for the DFF deployment as described above, the attitude of the remainder of the payload was changed to orient it in a magnetically east–west direction with the daughter at the western end of the payload, and the longitudinal axis parallel to the Earth's surface.

Once the daughter deployment attitude was achieved, all further maneuvers were roll maneuvers to produce a variety of sweeps in pitch angle for the MEG beams. The pitch-angle changes were to cause the beam to sweep through a predicted theoretical optimum pitch angle of ≈45 deg downward to provide the strongest source of vlf waves. The first of the roll maneuvers was performed before daughter deployment. The separation of mother and daughter then occurred at the end of sequence 1, and the next set of pitch angles was scanned. The pitch-angle scan periods were set to match the beam-emission–gas-discharge program of 32-s duration, described earlier. Details of the pitch-angle scans are shown in Fig. 6.

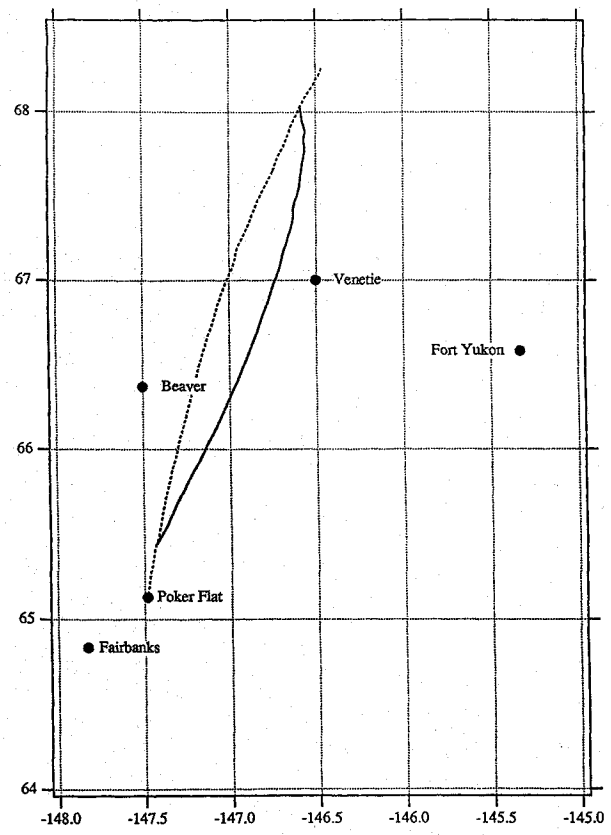


**Fig. 7 Map showing the locations of the launch site (Poker Flat) and the three vlf receiver sites at Beaver, Fort Yukon, and Venetie. The broken line shows the projection of the trajectory onto the ground, and the solid line shows the intersection of geomagnetic field lines at the trajectory with the ground.**

### vlf Ground Stations

Three downrange sites were selected to locate sensitive vlf receivers to attempt to detect electromagnetic wave signals at the modulation frequencies of the MEG beam. The sites were positioned at the nearest practical locations to the predicted footprints of vlf waves emerging from the ionosphere after being generated by the modulated electron beam, as shown in Fig. 7. All three sites were situated in the Yukon River valley near the villages of Fort Yukon, Venetie, and Beaver.

Receivers provided by the Stanford University group were located at Fort Yukon and Venetie, and additional receivers provided by Rome Laboratory were installed at Venetie and Beaver. The systems all used magnetic loop antennas feeding wideband vlf receivers, and the receiver outputs were recorded on magnetic tape at each site. The receiving systems were battery-operated, and they were able to operate for at least 2 h before recharging was necessary. Communication with the launch control at PFRR was mostly accomplished by public telephone, supplemented by a portable VHF radio link from the receiver site to the telephone location. At Fort Yukon extensive use was made of a telemetry link between the air base and PFRR.

### Optical Observations

Optical systems in support of the mission were set up at PFRR on the optical site supported by the Geophysical Institute of the University of Alaska, Fairbanks. Two LLLTV systems were attached to telescopes aimed at the predicted point of deposition of the beam energy in the E region. One of the two systems used the older image-orthicon detector technology; the other used an intensified CCD detector. The viewing directions were hand-steered using digital azimuth and elevation readouts that were offset from voiced information on the payload elevation and azimuth from the tracking radar. The field of view of the telescope was 12 deg. It was estimated that the size and intensity of the beam streak should be detectable against the star and auroral emission background under quiet auroral activity conditions.

An additional optical system at the range was a telescope with a photometer detector aimed at the predicted trajectory of the vehicle to search for emission from the beam and/or charge sheath near the mother section of the payload.

## Preliminary Results

### Beam Current

The two MEG units performed adequately throughout the time they were turned on during the flight. Figure 8 shows plots of the peak emission currents of each MEG as a function of mission elapsed time (MET). The general pattern of the data shows the implementation of the science timeline that required the gun to be on in groups of eight periods covering a time interval of 32 s, during which each of the four triads of frequencies was executed twice, once with the gas-release system on, then with it off.

Figure 8 shows that MEG 1 initially overperformed slightly, with peak emitted currents in the range 0.8–1.4 A, while MEG 2 underperformed, with peak emitted currents of 0.25–0.6 A. After the first science sequence, mother and daughter were separated, which resulted in excessive gas release due to the ACS compensating for a suspected tipoff that may have been caused by an incomplete electrical disconnect before the mechanical separation. The gas pressures close to the MEGs rose to a high enough level that excessive discharge currents flowed, and the automatic shutdown of the high voltage occurred. After the gas pressure returned to lower values as the ACS activity subsided, the MEGs continued to operate. MEG 2 now produced a constant peak current of about 0.6 A. MEG 1 was operating under space-charge-limited conditions and showed erratic behavior in the peak currents, which varied from 0.8 to 1.4 A over the mission. However, on the time scale of the ≈3 s periods while the MEG remained on for the emission of one of the triads of frequencies, the beam current showed much less variation.

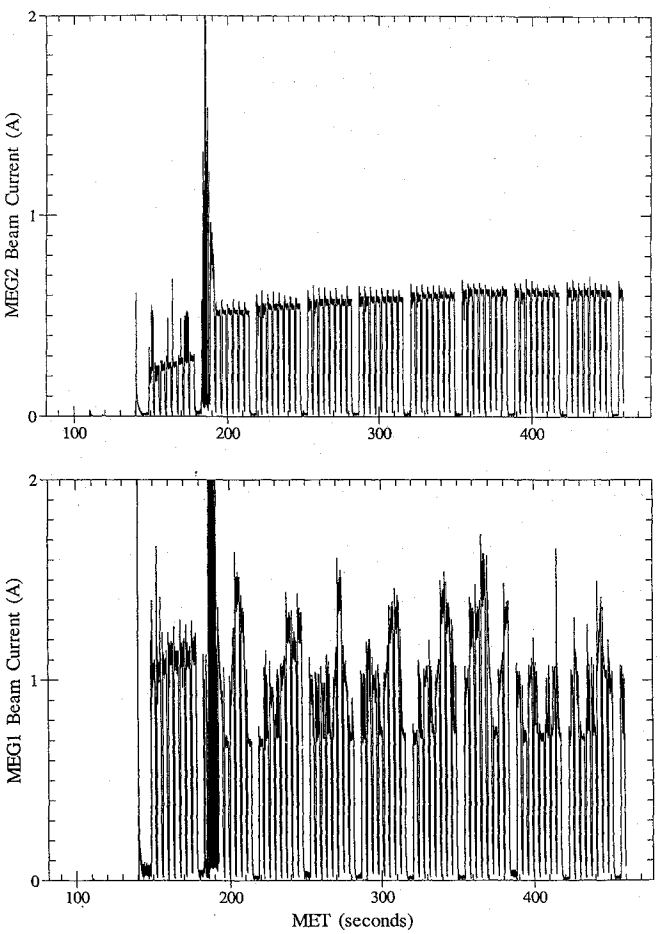


**Fig. 8 Plot of the measured beam currents for MEG2 and MEG1 against MET for the complete flight. The overall pattern shows the eight emission periods associated with each of the flight sequences.**

### Vehicle Charging, Emitted Energy

The electrical charging of the mother as a result of MEG electron-beam emissions was determined by measuring the voltage between the end of the tether connected to the deployed daughter and the ground of the mother. Since the electron emission drove the mother positive, the measured voltage had a negative polarity with reference to the payload ground. The accuracy of this measurement depends on the daughter structure remaining close to local ionospheric potential. This was achieved by using a high input impedance of 10 MΩ for the voltage-measuring circuit, and was checked by monitoring the tether current, which remained at an indicated zero throughout the flight.

One of the striking results seen in the vehicle potential data is the effectiveness of the gas-release system in reducing the mother potential from over 1000 V when the MEGs were operating without gas release to about 30 V when the gas was turned on. This result is illustrated in Fig. 9a, which shows the mother potential as a function of MET for sequence 5. The four gas-on periods are shown by the bars at the top of the figure, and it can be seen that this reduces the vehicle potential from over 1000 V to about 30 V. The noisy signals seen at times during this segment of data are a result of the ACS jets operating when the gas-discharge system is off. High-time-resolution plots of these noisy periods show that the vehicle potential is fluctuating from over 1000 V to 30 V at the ≈10-Hz pulsing frequency of the ACS jets. The times of electron-beam emission by the MEGs are shown by bars in Fig. 9, and the actual emission current profile for MEG1 for sequence 5 is shown in Fig. 9b. Close inspection of the vehicle charging shown in Fig. 9a indicates that there is charging, which is reduced whenever the gas release comes on when the MEGs are nominally in a nonemission state. This is due to a leakage beam current from the MEGs when the modulating signal is removed. This dc leakage was not detected by the Rogowski coil, and no direct means of measuring it in flight were available; however, based on laboratory tests, we believe the current level to be of the order of tens of milliamperes.

The effectiveness of the gas release in reducing the potential of the charged space platform supports earlier observations of ACS-induced lowering of the impedance between the vehicle and the ionosphere resulting from ionization of the gas cloud near the nozzle by the charged-particle flux returning to the electrically charged platform.[11,12]

The large reduction of vehicle potential associated with gas release resulted in an external beam energy at two different values. With the gas on, the emitted energy was close to the accelerated energy of 3000 V, but when the gas was off, the emitted energy was reduced by over 1000 V. Since the stimulation of the waves has been shown to be dependent on the emitted energy of the beam, the two modes will provide a useful variable in the analysis of the wave data.

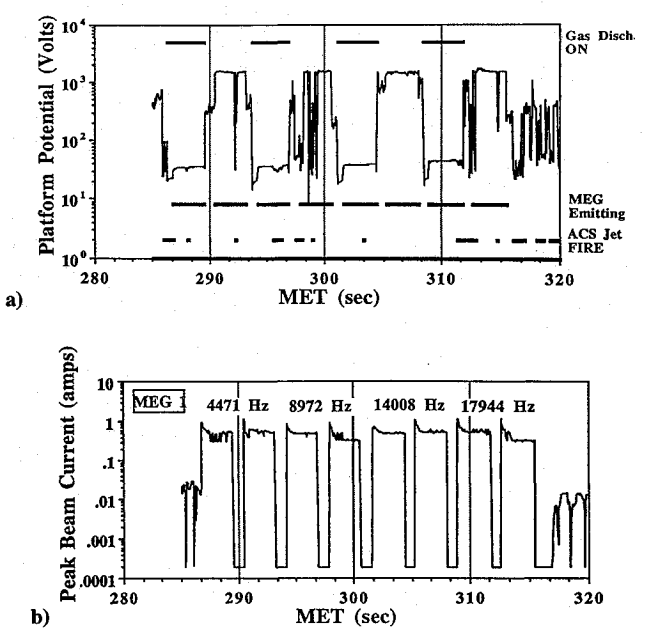


**Fig. 9 Plot of a) measured mother potential and b) MEG1 current as a function of MET for sequence 5. The periods of beam emission, programmed gas release, and ACS gas release are indicated by the bars.**

### Wave Detection

*At Daughter*

The HF and vlf receivers in the daughter section of the payload both responded to the active experiments being performed on the mother payload. The vlf automatic-gain-control level was high for all MEG emissions, although it has not yet been determined how much of the signal was collected by the tether acting as an antenna, and how much was directly radiated to the daughter. The high impedance between the tether and the mother ground should effectively decouple the tether from fluctuations in the mother ground potential. The background level of the vlf increased after the separation of the daughter from the mother. The level decreased when the tether wire was cut, which indicates that it acted as a vlf antenna for the background waves.

Figure 10 shows the dynamic power spectrum of three successive sequences as a function of gun modulation frequency. The modulation bursts start at 150-s MET (a), at 250-s MET (b), and at 430-s MET (c). To the right of the frequency spectra, the duration

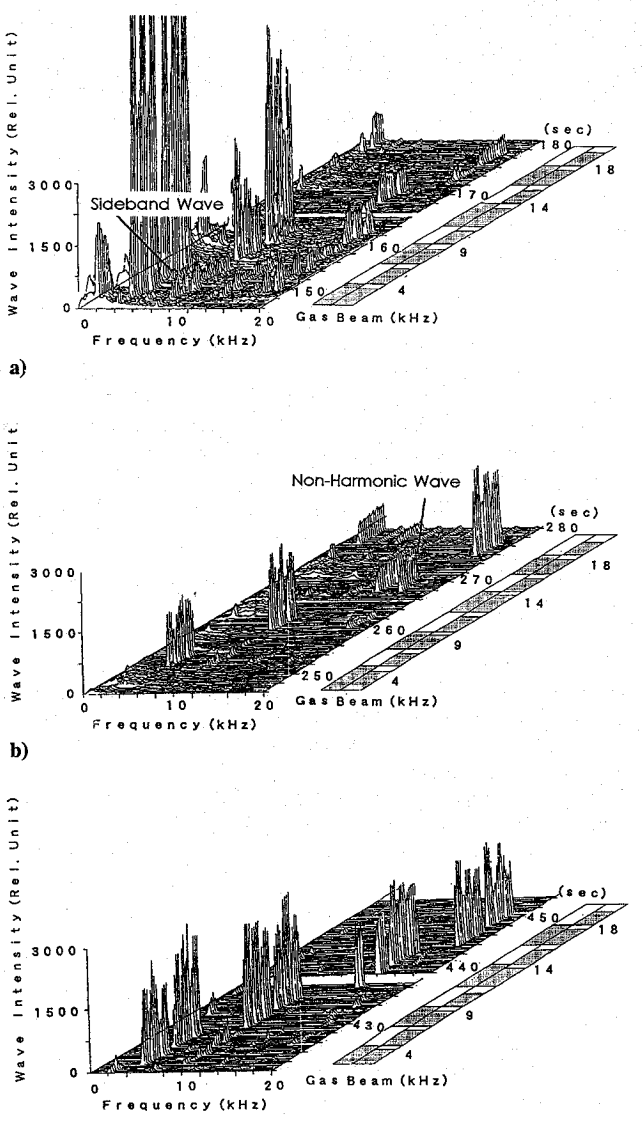


**Fig. 10 Plot of a series of derived power spectra from the daughter broadband vlf receiver for three frequency programs with and without programmed gas release at early, mid, and late flight times. The power spectral density is in arbitrary units, and the time scale is MET.**

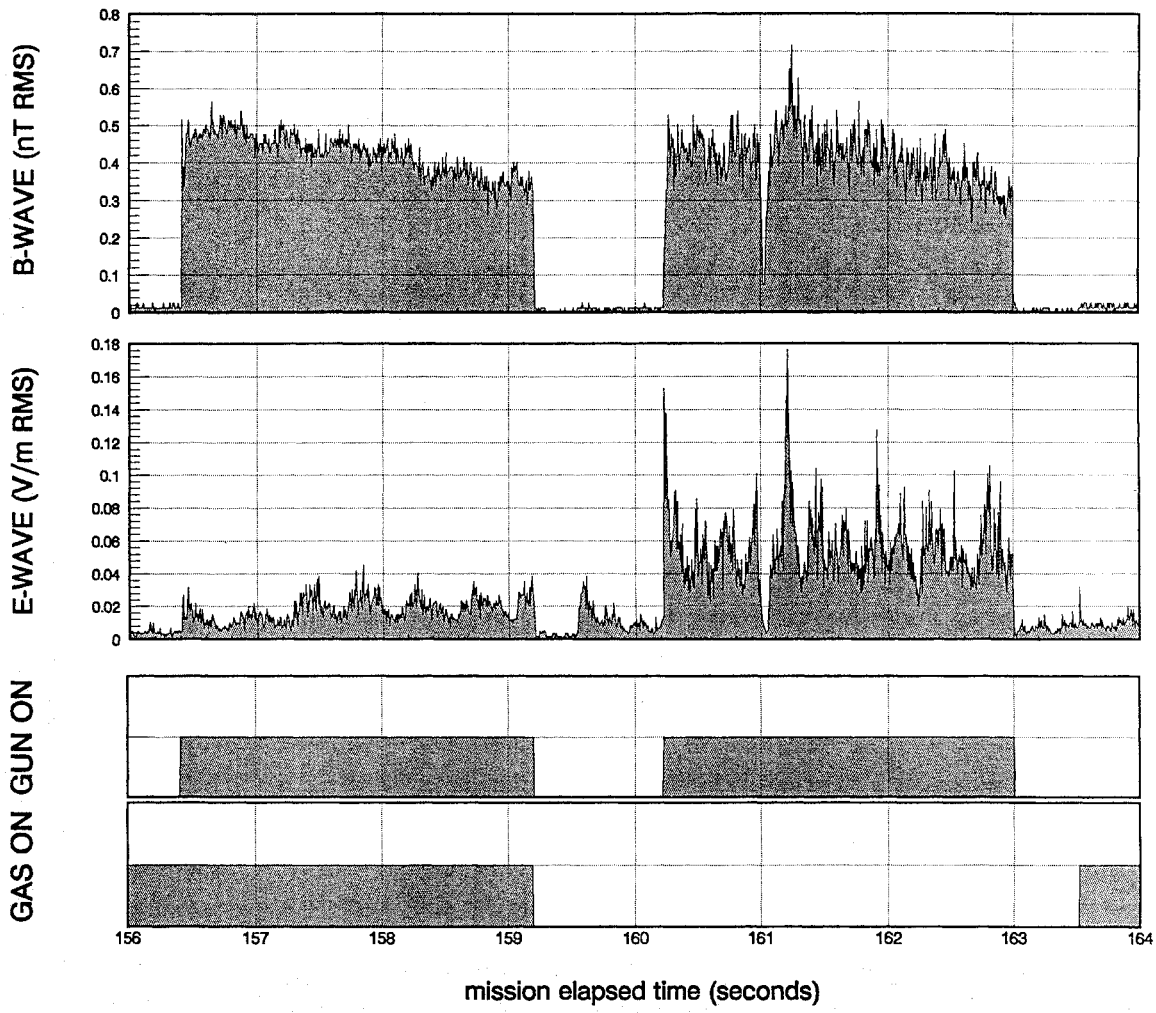


**Fig. 11 Plots of the total E- and B-wave intensities against MET during a beam modulation at 8970 Hz from the DFF vlf receiver with and without programmed gas release. The timing of the gas release and the beam emission are shown in the lower panels of the plot.**

of the gas releases and MEG emission, times are shown. During the MEG emissions, strong fundamental waves and harmonics were generated. A weak wave was found to be generated close to 4 kHz when the gas release was inhibited (indicated as a sideband in Fig. 10a), which might be the result of a nonlinear beam–plasma interaction. The intensity of these MEG-related waves was greatly reduced when the gas-release system was on, which might mean that the waves were attenuated by collisional damping. This trend was observed throughout the flight.

*At DFF*

The DFF wave instruments provided clear evidence of wave signals from its initial release through the end of the operational part of the flight. One of the early observations was that the presence of the gas emitted by the gas-release system had a marked effect on the wave signals detected by the DFF instruments.

Figure 11 shows plots of the total wave energy in the electric and magnetic components for the 8970-Hz modulation with and without neutral-gas release. The MET of these data is early enough that the separation of the daughter from the mother is only about 220 m. The plot shows that the total wave energy of the magnetic component is hardly affected by the presence of the gas, but there is a large increase in the average wave intensity of the electric component when the gas flow was off. The high electric field component may be evidence of electrostatic wave instabilities predicted by numerical modeling of the beam–environment interaction, which are enhanced by the lower beam neutralization in the higher vacuum and the greater degree of vehicle charging observed to occur when the gas release is inhibited.[13,14]

Some feeling for anomalous beam–environment interaction can be obtained of the detected wave signals. Figure 12a shows the surprising result that at the 200-m range the presence of harmonics of the 8970-Hz modulation frequency is clearly seen in both the electric and magnetic components of the detected waves. This harmonic generation was also affected by the gas release, being less apparent in both wave components when the gas release was off, as shown in Fig. 12b.

Spectra of the waves much later in the flight, when the DFF–mother separation was about 1500 m, still show the presence of the harmonics in the magnetic component, but they are not discernible in the electric component.

*On Ground*

The initial frequency analysis of the tapes recorded by the ground stations did not show any obvious evidence of signals from the modulated beam above the local noise levels propagating to the ground sites. The data were analyzed using spectral analysis equipment, and further studies are to be made using digitization of data segments concurrently with the modulation periods to establish the upper limit of the intensities of the emitted waves.

**Ground-Based Optical Observations**

No evidence of light resulting from beam-induced ionization of the atmosphere was observed during most of the flight. Because of a late call on the flight path from the tracking radar, the LLLTV cameras were aimed low during much of the flight. However, seven periods were identified during which artificial auroral streaks should have been within the field of view of the cameras. The observing

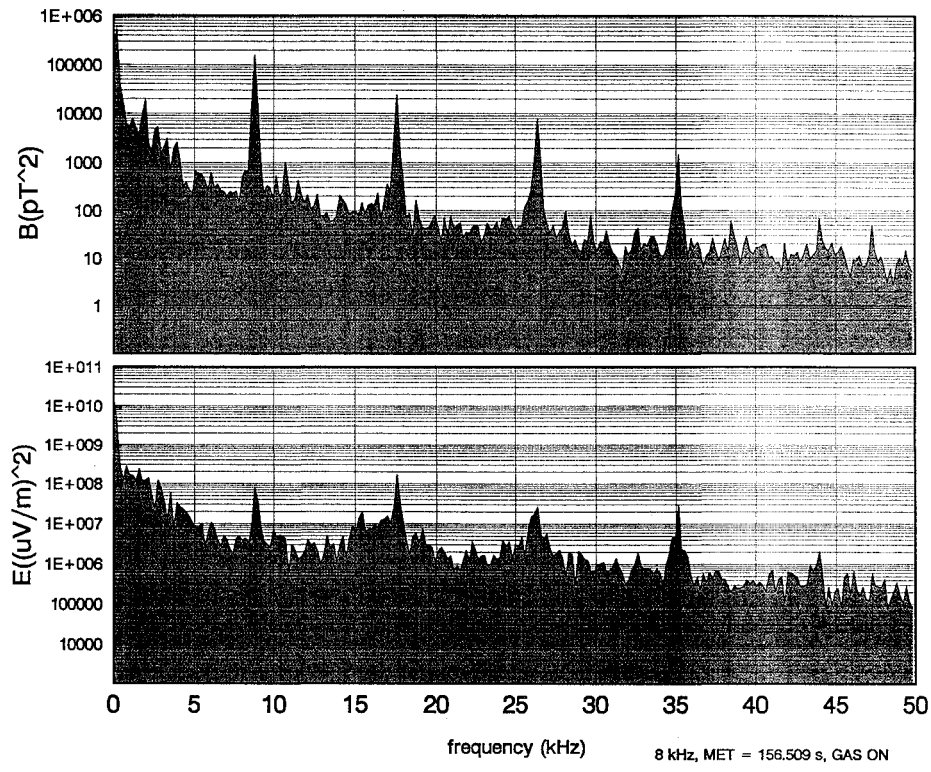


a)

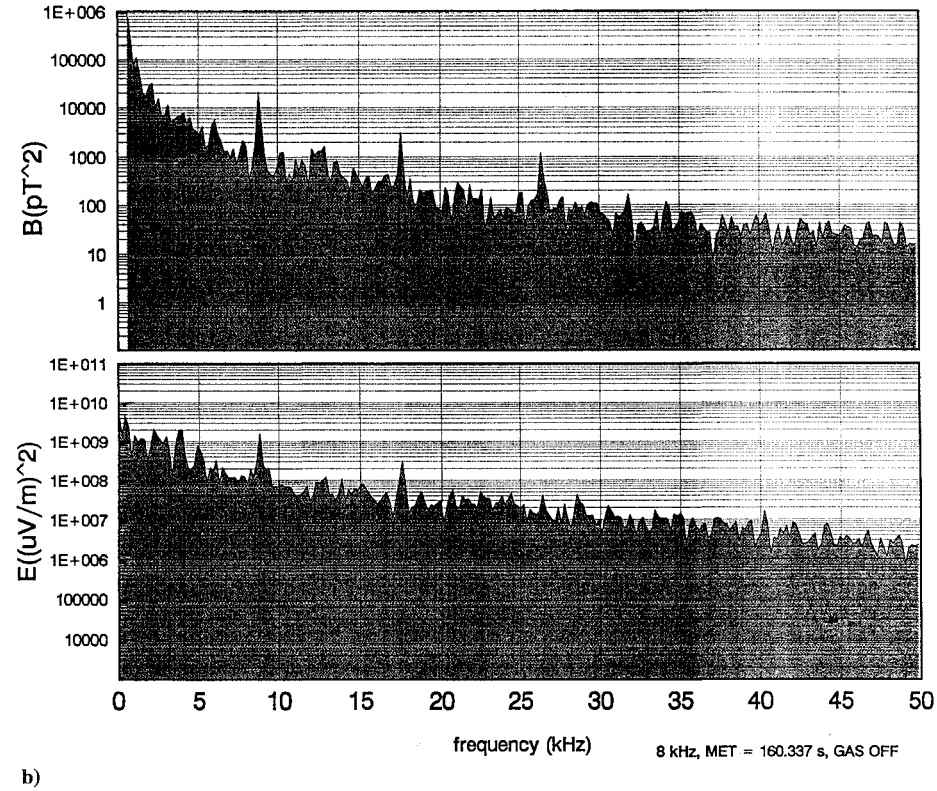


b)

**Fig. 12 Plot of the power spectrum of the B- and E-wave fields detected by the DFF vlf receiver for a beam modulation frequency of 8970 Hz: a) at 156-s MET when the programmed gas release was on and b) at 160-s MET when the programmed gas release was off.**

conditions were degraded somewhat by the presence of the 2-kR (5577-Å) diffuse natural aurora. On the basis of the observed limiting magnitude of 8.0 in single-frame TV images, and comparison with the ECHO IV results, it is estimated[15] that the peak current required for threshold visibility of the artificial aurorae under these conditions would have been 1.6 A. It happens that most of the pulses were just below this value, as shown in Fig. 8.

At MET 466 s (116-km altitude), a streak was observed to extend a few kilometers from the payload. This is consistent with expectations for 3-keV electrons, and confirms that the beam escaped from the immediate vicinity of the payload at that altitude.

The photometer data produced no evidence of light emission from the vicinity of the payload.

## Summary and Conclusions

The flight of the CHARGE-2B payload as part of NASA sounding-rocket mission 39.003 was successful. All instruments in space and those forming the ground support element of the project were operational and performed at or close to specifications. The mechanical aspects of the flight, including the boost phase, door deployments, subsystem deployments, attitude maneuvers, and recovery systems, functioned correctly. The electrical operation of the payload was nominal, and all support systems such as power, sequencing, and telemetry worked well. The ground system support functions were good, with complete recovery of telemetry and good radar tracking of the payload.

Scientifically we expect large returns from the data obtained by this flight. The wave measurements near the payload on the scales of hundreds of meters and of kilometers will yield important information on beam–environment interactions and on the ability of the beam to act as an antenna launching electromagnetic waves. The lack of detection of waves at the ground, compounded with estimations of the source function of the waves from the nearby measurements, will either validate the source and ray-tracing models used, or point to adjustments to be made to the theory.

The other important scientific result from the flight relates to the use of gas release as a method of grounding positively charged space platforms. The gas releases coordinated with the electron-beam emissions provided clear evidence of the ability of this technique to reduce the potential of the platform to tens of volts above the ambient ionospheric potential. The serendipitous operation of the ACS during periods when the vehicle was charged supports the conclusions obtained from the gas-release system, and, in addition, provides data to explore the transient behavior of gas releases in controlling the grounding and recharging of the electrical potential of the vehicle.

## Acknowledgments

This project was supported by NASA Grants NAG5-607, NAG5-658, and NAGW 1817 to Utah State University and by Rome Laboratory Contracts F19628-91-K-0037 to USU, F19628-89-K-0040 to Stanford University, and F19628-91-K-0035 to the University of Alaska. We would like to thank the many engineers and technicians at USU/SDL, ISAS, Rome Laboratory, Wallops Flight Facility, and PFRR, all of whom contributed to make the mission a success. In particular we thank David Kotsifakis of WFF and Ron Pierce of PFRR, who managed the NASA operations at the integration facility and the range. Several theorists helped to define the frequencies and ground locations of the vlf receivers, and we would like to acknowledge in particular the assistance of Peter M. Banks, Ken Harker, and Torsten Neubert. We are grateful to Donald C. Thompson for adapting his general-purpose data-handling and graphics programs to speed up the data reduction. We would also like to recognize the vision of the late Stanley Shawhan of NASA Headquarters, who recognized the value of the space environment as a place to perform unique physics experiments, and the practicality of combining NASA resources with those of other agencies to accomplish projects that would otherwise have languished through lack of funding.

## References

[1]Beard, D. B., and Johnson, F. S., "Ionospheric Limitations on Attainable Satellite Potential," *Journal of Geophysical Research*, Vol. 66, 1961, pp. 4113–4120.

[2]Hess, W. N., Trichel, M. G., Davis, T. N., Beggs, W. C., Kraft, G. E., Stassinopoulos, E., and Maier, E. J. R., "Artificial Auroral Experiment: Experiment and Principal Results," *Journal of Geophysical Research*, Vol. 76, 1971, pp. 6067–6074.

[3]Winckler, J. R., "The Application of Electron Beams to Magnetospheric Research," *Reviews of Geophysics and Space Physics*, Vol. 18, 1980, pp. 659–670.

[4]Wilhelm, K., Bernstein, W., Kellogg, P. J., and Whalen, B. A., "Acceleration of Electrons in Strong Beam–Plasma Interactions," *Geophysical Research Letters*, Vol. 11, 1984, pp. 1176–1178.

[5]Lavergnat, J., "The French-Soviet Experiments ARAKS: Main Results," *Artificial Particle Beams in Space Plasma Studies*, Plenum, New York, 1982, pp. 87–100.

[6]Maehlum, B. N., Maeseide, K., Aarsnes, K., Egeland, A., Grandal, B., Holtet, J., Jacobsen, T. A., Maynard, N. C., Sorass, F., Stadsnes, J., Thrane, E. V., and Troim, J., "POLAR-5—an Electron Accelerator Experiment Within an Aurora: 1. Instrumentation and Geophysical Conditions," *Planetary and Space Science*, Vol. 28, 1980, pp. 259–272.

[7]Myers, N. B., "Studies of the System–Environment Interaction by Electron Beam Emission from a Sounding Rocket Payload in the Ionosphere," Ph.D. Dissertation, Utah State Univ., 1989.

[8]Myers, N. B., Raitt, W. J., White, A. B., Banks, P. M., Gilchrist, B. E., and Sasaki, S., "Vehicle Charging Effects During Electron Beam Emission from the CHARGE-2 Experiment," *Journal of Spacecraft and Rockets*, Vol. 27, 1990, pp. 25–37.

[9]Lavergnat, J., Le Queau, D., Pellat, R., Roux, A., and Saint Marc, A., "Electron Beam as a Source of Electrostatic Waves," *Artificial Particle Beams in Space Plasma Studies*, Plenum, New York, 1982, pp. 525–534.

[10]Holtzworth, R. H., and Koons, H. C., "VLF Emissions from a Modulated Electron Beam in the Auroral Ionosphere," *Journal of Geophysical Research*, Vol. 86, 1981, pp. 853–857.

[11]Gilchrist, B. E., Banks, P. M., Neubert, T., Williamson, P. R., Myers, N. B., Raitt, W. J., and Sasaki, S., "Electron Collection Enhancement Arising from Neutral Gas Jets on a Charged Vehicle in the Ionosphere," *Journal of Geophysical Research*, Vol. 95, 1990, pp. 2469–2475.

[12]Gilchrist, B. E., "Measurements of Electron Beam and Neutral Gas Emissions in a Space Plasma During an Ionospheric Modification Experiment," Ph.D. Dissertation, Stanford Univ. Stanford, CA, 1991.

[13]Winglee, R. M., and Pritchett, P. L., "Comparative Study of Cross-Field and Field Aligned Electron Beams in Active Experiments," *Journal of Geophysical Research*, Vol. 93, 1988, pp. 5823–5830.

[14]Pritchett, P. L., "A Three-Dimensional Simulation Model for Electron Beam Injection Experiments in Space," *Journal of Geophysical Research*, Vol. 96, 1991, pp. 13781–13793.

[15]Hallinan, T. J., Stenbaek-Nielsen, H. C., and Winckler, J. R., "The ECHO-4 Electron Beam Experiment: Television Observations of Artificial Auroral Streaks Indicating Strong Beam Interactions in the High-Latitude Magnetosphere," *Journal of Geophysical Research*, Vol. 83, 1978, pp. 3263–3267.

A. L. Vampola
*Associate Editor*